Received: 31 October 2021 | Revised: 22 January 2022 | Accepted: 19 March 2022

DOI: 10.1002/stc.2973

RESEARCH ARTICLE

WILEY

Novel magnetic levitation systems for the vibration control of lightweight structures and artworks

Filipe Amarante dos Santos[1] | **Fernando Fraternali**[2]

[1]CERIS, Department of Civil Engineering, NOVA School of Science and Technology, Universidade NOVA de Lisboa, Caparica

[2]Department of Civil Engineering, University of Salerno, Fisciano, Italy

Correspondence
Filipe Amarante dos Santos, CERIS, Department of Civil Engineering, NOVA School of Science and Technology, Universidade NOVA de Lisboa, 2829-516 Caparica, Portugal.
Email: fpas@fct.unl.pt

Funding information
Ministero dell'Istruzione, dell'Università e della Ricerca, Grant/Award Number: 2017J4EAYB; Università degli Studi di Salerno

Abstract

This work designs, models, and experimentally validates novel magnetic levitation systems for the vibration isolation of lightweight structures and artworks. 2D and 3D passive vibration isolators are studied, making use of easy-to-assemble 3D-printed components and neodymium magnets. An optimized design of the number of magnets and the 3D printing process of the stabilizing parts allows us to finely tune the resonant frequencies and the vibration isolation performances. Ratios between the maximum horizontal and vertical accelerations, exhibited by the floating bodies, and the maximum horizontal acceleration applied to the base of the system are provided, for varying excitation frequencies. With these outputs, we show that it is possible to optimize the main design parameters of the isolation system, by targeting the desired frequency window, for a given payload.

KEYWORDS

additive manufacturing, artworks, lightweight structures, maglev, vibration isolation

1 | INTRODUCTION

The design of vibration isolation systems for lightweight structures cannot be easily achieved by scaling down the conventional vibration isolation systems used for civil engineering structures and mechanical equipment (refer, e.g., to previous works[1,2] and references therein). Several different types of innovative devices and metastructures are currently being studied to protect the non-structural components of buildings (precision machinery, vibration-sensitive equipment in essential buildings, artworks in museums, etc.), which are exposed to earthquakes, traffic noise, and different sources of low-frequency vibrations.[3–5]

The protection of artworks in museums and art exhibitions exposed to vibration loading is of special importance, due to the great and often inestimable value of statues and other artworks stored in such venues (see the comprehensive literature review presented in literature[6]). These museum pieces typically respond to vibration excitations as rigid systems, exhibiting rocking and sliding motions.[6,7] Available literature studies in this field have shown that rubber-bearings are not convenient for the seismic isolation of lightweight artworks,[2] while effective isolation devices are offered by rolling ball systems,[2] friction pendulum bearings,[7,8] active control systems,[6] and devices based on shape memory alloy wires.[9] Instead of protecting a single artwork, it is also possible to isolate the entire floor of a museum or an essential building, through conventional or low-cost techniques.[10,11]

Over the past few years, various authors have been investigating magnetic levitation ("maglev") systems, namely, for vibration damping and isolation purposes. These systems are of particular interest due to their ability to provide extremely low isolation stiffness and very high isolation efficiency, even in the presence of low-amplitude excitations.[12–15] Passive electromagnetic devices for vibration damping and isolation are becoming a real alternative to traditional mechanical vibration and isolation methods. Passive devices, like Eddy current dampers, can be designed to mitigate vibrations without the need of active feedback and control. These devices show overall good damping capabilities, low cost, null power consumption, and high reliability.[16–18] Tsuda et al. have proposed maglev isolation devices that couple bulks made of high-temperature superconducting (HTS) magnets with permanent magnets (PMs).[12,13] When used in appropriate arrangements, it has been shown that such systems can effectively mitigate horizontal[12] and vertical[13] vibrations. However, HTS-based maglev systems show important shortcomings when compared with alternative systems that rely on magnetic damping at room temperature, namely, the fact that they need cooling. Sasaki et al[14] showed that the levitation force of such systems is high enough for very small gaps between HTS bulks and PMs and that the magnitude of such a force shrinks in the case of larger gaps. This issue implies that the arrangement of the magnets is a crucial feature and that the cooling system of the HTS bulks may significantly affect the size of the gap. Other available maglev isolators make exclusive use of PMs, introducing the concept of magnetic springs.[1,15] Kumar et al have proposed a PM isolation system that becomes active and lifts the structure to be isolated in the presence of seismic waves, and which returns to off mode when the earthquake is over. Of course, such a system needs vibration sensors to sense the ground oscillation and activate the levitation mechanism. Frizenschaf et al[1] have developed a maglev isolator that uses inclined PM springs, while Yao and Huang[15] have used magnetic springs within a guideway sliding isolator for precision machinery. A key advantage of such systems is the independence of the resonating frequencies from the payload masses, as opposed to linear mechanical springs. However, one challenge to be addressed is the stability of the levitating structure, which is not an easy task in terms of all the translational and rotational vibration modes.[1] According to Earnshaw's theorem,[19] it is indeed not possible to obtain a stable stationary equilibrium configuration solely through the interaction of magnetic forces due to PMs. This means that PM systems need to make use of suitable mechanical constraints to ensure stability.[1,15]

The present work develops and experimentally characterizes novel and tunable maglev systems that passively attenuate horizontal vibrations applied at the base of the system. The proposed devices assemble PMs and additively manufactured components, making use of standard 3D printing techniques based on fused deposition modeling (FDM) and environmentally sustainable materials. The proposed systems take advantage of the high magnetic forces delivered by neodymium magnets and the stiffening effects of 3D-printed components to design stable levitating platforms. Neodymium magnets (also known as NdFeB, NIB, or Neo-magnets) are the most widely used type of rare-earth magnets today.[20] These PMs are made from an alloy of neodymium, iron, and boron to form the $Nd_2Fe_{14}B$ tetragonal crystalline structure. The proposed maglev systems do not require either the use of sub-zero temperatures, like in the case of maglev systems based in superconducting materials, or electrical power, like in electromagnetic systems. Stabilizing systems are provided by 3D-printed elements exhibiting stiffness that can be effectively tailored to the frequency content of the prescribed loading and the payload. Distinctive features of the isolators developed in the present work are their ease of manufacture using standard 3D printers, sustainable FDM materials, and low-cost magnets provided by online suppliers available all over the world; the tunability of the stabilization system and the resonant frequencies made possible by an optimized design of the 3D printing process of the stabilizing parts; and their unprecedented application for the vibration isolation of artworks. The first analyzed maglev system attenuates vibrations in a plane, due to the presence of out-of-plane restraining plates (2D system). A 3D system mitigates arbitrarily directed horizontal vibrations and vertical vibrations of a floating artwork mock-up subject to horizontal accelerations at the lower base. The given results illustrate how the ratios between maximum horizontal and vertical accelerations of the floating bodies and the maximum horizontal acceleration applied at the base of the system can be finely tuned through an optimized design of the system components.

2 | MATERIALS AND METHODS

2.1 | Magnetic force characterization

We used CS-S-34-04-N countersunk neodymium disk magnets, with a diameter of 34 mm, thickness of 4 mm, weight of 26 g, and material properties given in Supporting Information Text.

A Zwick/Roell Z50 universal testing machine operating at the strain rate of 0.1%/s was employed to characterize the nonlinear relationship between the repulsive magnetic force and the distance between the magnets. The magnets were screwed into two specially designed base plates placed between the grips of the testing machine (see Figure 1). Figure 2 illustrates the experimentally recorded curve relating the repulsive force F versus the distance (or gap) d between the magnets.

The maximum repulsive force F recorded between the two magnets was approximately equal to 70 N, in correspondence with the configuration showing a 1 mm gap d between the magnets. As the gap increased, the magnetic force decreased according to the nonlinear $F-d$ curve shown in Figure 2. The magnetic force was approximately zero when the distance between the surface of the magnets was higher than 40 mm.

2.2 | Design of maglev isolation systems

2.2.1 | Planar system

A first version of the proposed maglev system is aimed at isolating vibrations while the base of the system is excited by a horizontal acceleration record. The 2D system is composed of the following main parts: (i) a levitating platform; (ii) a floating cylinder; (iii) a base platform; (iv) confinement plates/walls restraining out-of-plane vibrations; and (v) a stabilizing system composed of 3D-printed strips (Figure 3). Two couples of repelling disk magnets are employed to separate the levitating platform from the base of the device. The system is designed to allow the levitating platform to move along its longitudinal and vertical axes, being restrained by confinement walls in the transverse direction. Both platforms were 3D printed using eco-sustainable polylactic acid (PLA) filaments for FDM (see Supporting Information Text for the details of the 3D printing process). The horizontal stabilization system comprises two antagonistic "FLEX" strips, which were also 3D printed using a thermoplastic polyether-polyurethane elastomer. These strips connect the

FIGURE 1 Experimental setup for the magnetic force–distance characterization. (a) Front view of the configuration with the magnets. (b) 3D view

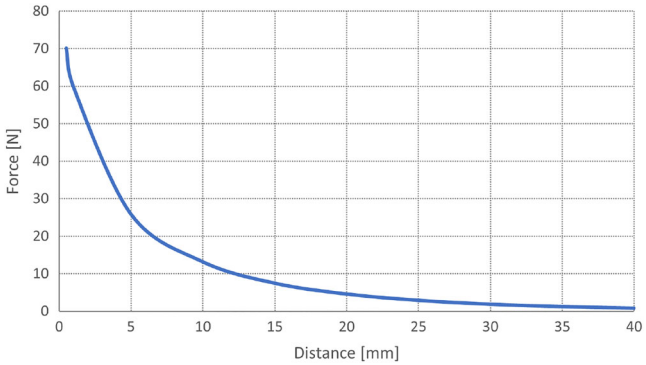

FIGURE 2 Experimental characterization of the magnetic force versus distance relationship

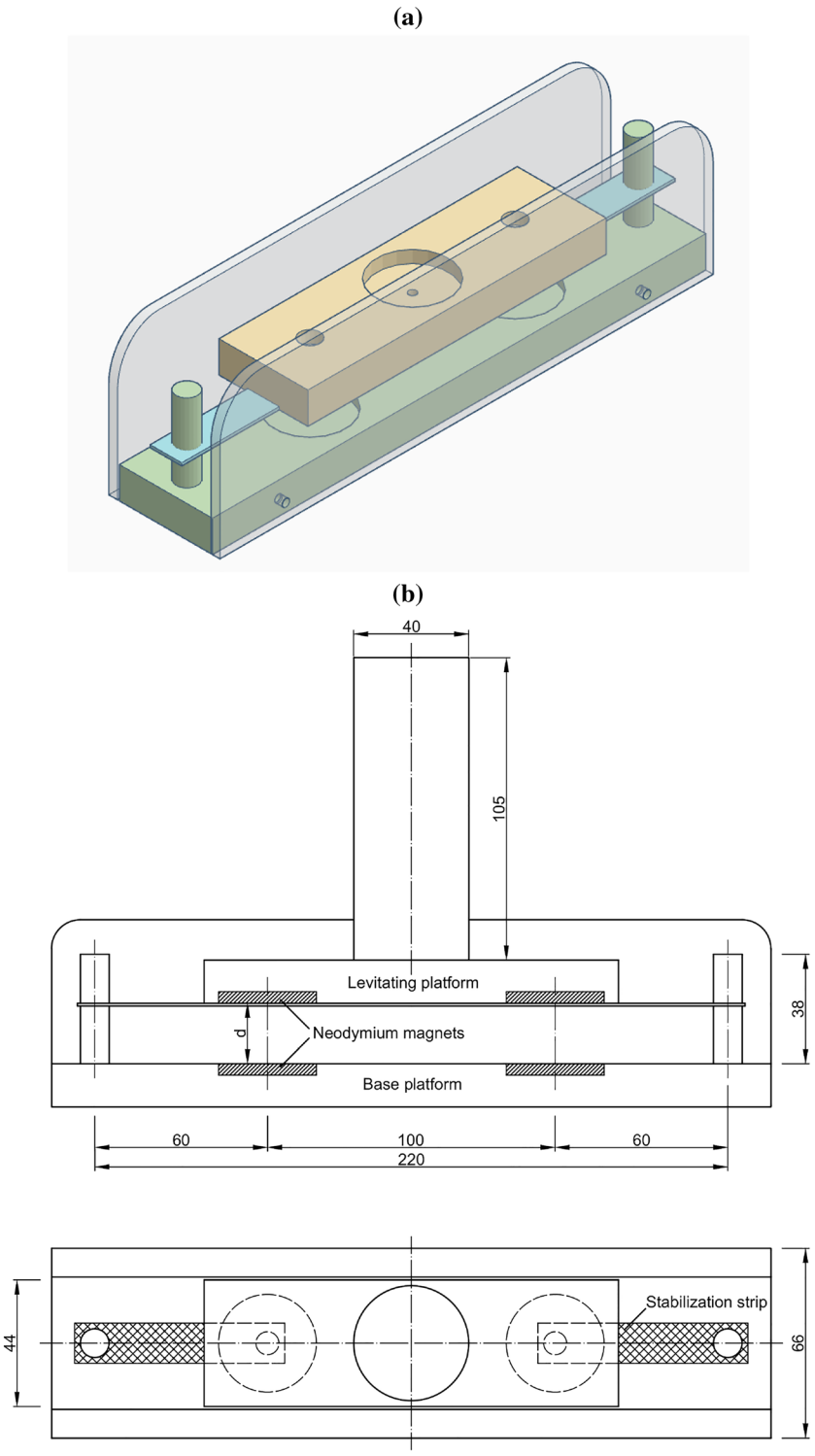

FIGURE 3 Illustration of the 2D maglev system. (a) CAD model. (b) Technical drawings: lateral and top views (all dimensions are in mm)

levitating platform to the base platform through two vertical cylindrical posts, placed at the extremities of the base platform. The horizontal stabilizing strips are fixed to the levitating platform at one end and can be horizontally leveled by moving the opposite end along the cylindrical posts, through specially designed circular holes. Since we place the strips horizontally, they provide very little vertical stiffness to the maglev isolator. As a result, it is possible to uncouple the vertical and horizontal motions of the levitating platform. The isolated body consists of a hollow cylindrical capsule,

with a height of 105 mm and diameter of 40 mm, filled with stacked steel spheres which are covered by a top lid. The computer-aided design (CAD) model and a technical drawing of the 2D prototype are shown in Figure 3a,b, respectively. As Figure 3b shows, two lateral plates guide the top platform to move either along its longitudinal direction or in the vertical direction, by preventing transverse motions and rotations about the longitudinal axis. The magnets are nested inside the two platforms and are fixed with countersunk screws. The floating cylinder is screwed to the center of the levitating platform. The overall weight of the cylinder and the levitating platform is 0.493 kg. The horizontal stiffness of this platform can be tailored through a suitable design of the FLEX stabilization strips, which are 15 mm wide and 1 mm thick. Three different designs of such strips were considered, by setting the infill density of the pattern used to 3D print such elements to 15% (type A), 20% (type B), and 25% (see Supporting Information Text for the details of the examined physical model, and a graphic illustration of the stabilization strips, Figure S2).

2.2.2 | Three-dimensional system

A three-dimensional maglev system was designed to isolate the vibrations of objects like artworks along three mutually perpendicular axes, while applying a horizontal acceleration record to the lower base of the device. The 3D system is equipped with two platforms shaped as regular octagons that feature a side length of 80 mm and indentations along the sides. These platforms can incorporate up to nine CS-S-34-04-N neodymium disk magnets each (Figures 4 and 5). The stabilization system of the levitating platform uses a 3D-printed FLEX membrane with octagonal shape (side length of

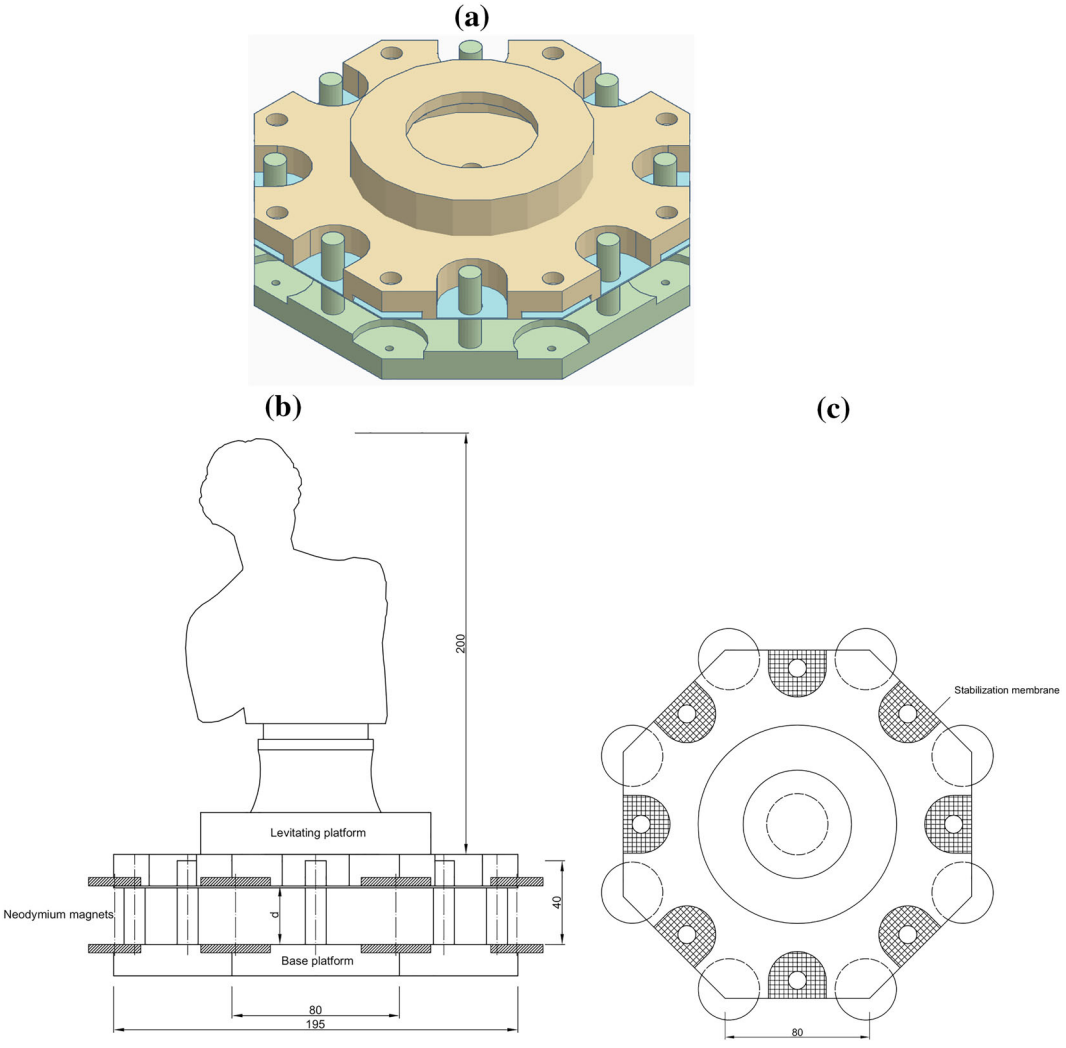

FIGURE 4 Illustration of the 3D maglev system. (a) CAD model. (b) Lateral view. (c) Top view (all dimensions are in mm)

80 mm; 1 mm thickness) of two different types, which stabilizes the system in all directions of the horizontal plane (see supporting information for further details). Type A membrane was 3D printed using an infill density of 20%, while type B used a 40% infill density. The stabilizing membrane lies at the bottom of the levitating platform. As in the 2D case, the levitating platform is free to move in the vertical direction. It indeed shows circular holes that can slide along eight cylindrical posts running within the indentations of the top plate (Figure 4). A mock-up of the bust statue of Venus de Milo, which is 200 mm tall and weights 1.0 kg, was fixed to the levitating platform (Figure 4). By changing the number of disk magnets, it is possible to tailor the height of the levitating platform and the stiffness of the maglev system, according to the particular problem at hand. We tested the two alternative configurations, shown in Figure 5, with four and nine pairs of magnets, weighting 0.1104 and 0.1234 kg, respectively.

2.3 | Shake-table setups

A commercial shake-table Quanser Shake-Table II was used to excite both the 2D and 3D maglev prototypes, which were equipped with three PCB Piezotronics, Inc. accelerometers, model 33B42, connected to a NI SCXI-1530 4-channel accelerometer amplifier. The employed data acquisition platform was NI PXI-1052. A DAQ assistant express VI, using NI-DAQmx software, was used to create, edit, and run the analog inputs corresponding to the voltage measurement tasks. Two accelerometers were placed on top of the floating bodies, to measure horizontal and vertical accelerations, while a third accelerometer was attached to the shake-table to record the applied horizontal acceleration history. For the 2D system, the levitating height at rest position was 27 mm. Figure 6a,b shows two different views of this maglev prototype mounted on the shake-table. In the case of the 3D system, the levitating height at rest position of the statue mock-up was equal to 25 and 33 mm for the four and nine magnets configurations, respectively. Figure 6c–e illustrates different views of the 3D maglev prototype under testing (see supporting information for additional details).

3 | RESULTS AND DISCUSSIONS

3.1 | Results for the 2D system

3.1.1 | Modal analysis

A finite element (FE) analysis of the 2D system was performed through the model presented in Figure S3, in order to estimate the fundamental vibration modes and the associated vibration frequencies. The first three vibration modes obtained from the FE analysis are presented in Figure 7. Table 1 gives the natural frequencies of such modes, for the three different designs of the stabilization strips. Mode 1 corresponds to a pure rocking motion with a pivot point at the middle of the levitating platform. Mode 2 is a pure vertical motion. Mode 3 is a combined rocking-sliding motion.

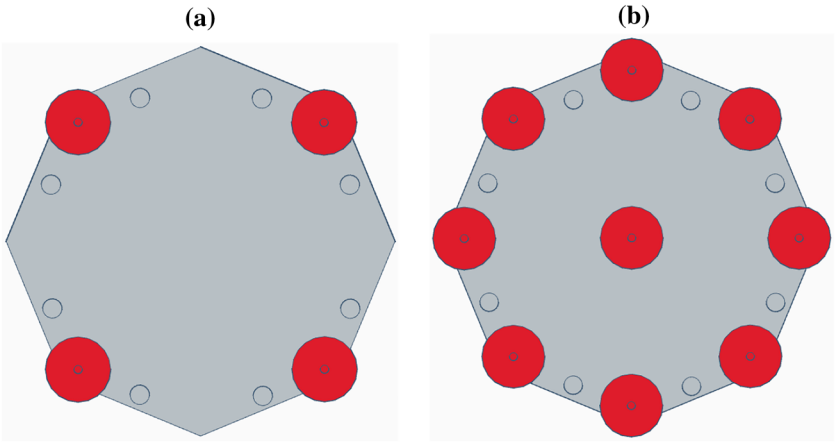

FIGURE 5 Different configurations of the disk magnets for the 3D maglev system. (a) Four pairs of magnets. (b) Nine pairs of magnets

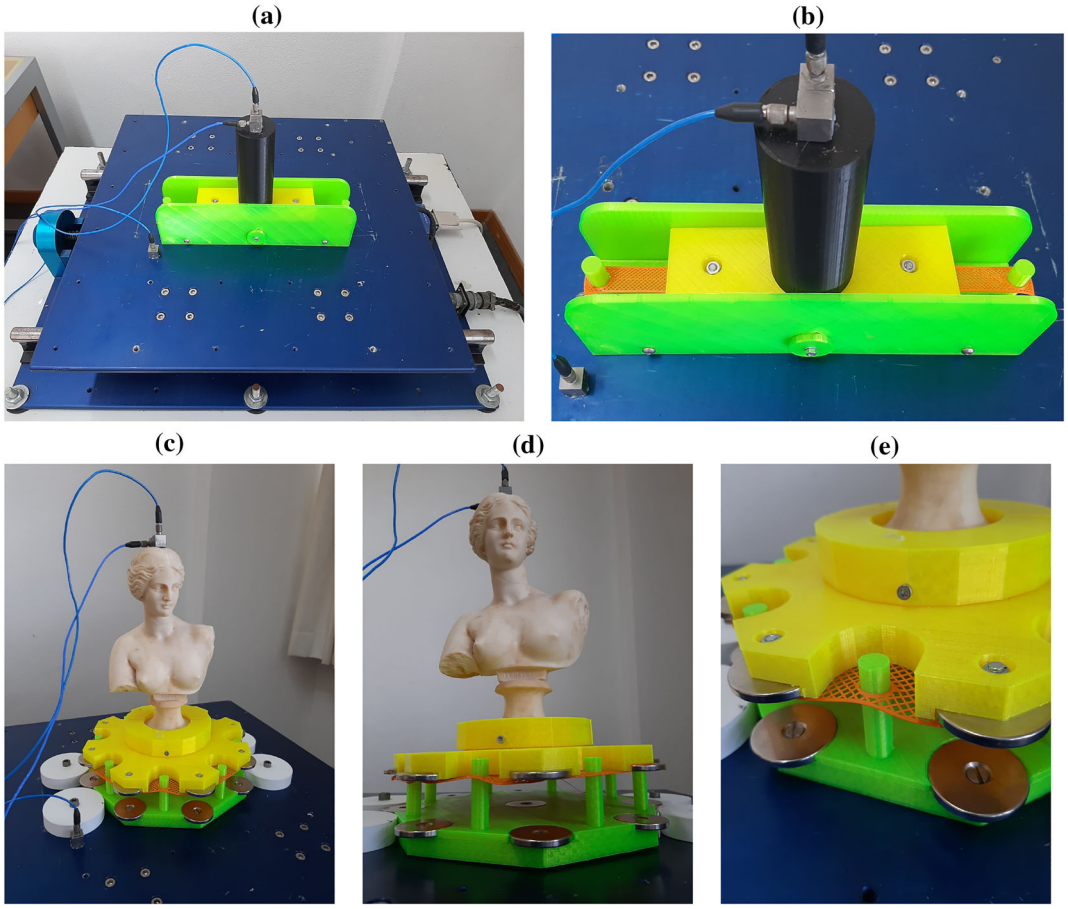

FIGURE 6 Shake-table setups. (a) 2D maglev prototype mounted on the shake-table. (b) Close-up detail of the 2D prototype under testing. (c,d) Statue mock-up mounted on the 3D maglev prototype resting on the shake-table. (e) Close-up detail of the platforms of the 3D prototype under testing

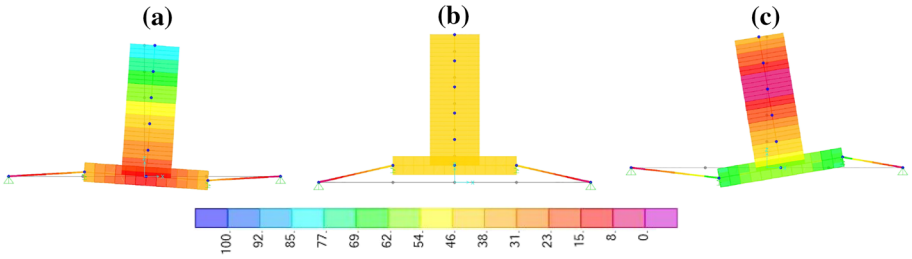

FIGURE 7 Modal configurations for the first three vibration modes of the 2D system. (a) First, pure rocking mode. (b) Second, vertical mode. (c) Third, mixed rocking-sliding mode

TABLE 1 Natural frequencies associated with the vibration modes in Figure 7

Strip	Mode 1 freq. (Hz)	Mode 2 freq. (Hz)	Mode 3 freq. (Hz)
A	3.9	5.3	9.9
B	4.0	5.3	11.2
C	4.1	5.3	12.4

The contribution of the horizontal stabilization strips to modes 1 and 2 is rather limited, as illustrated by the results presented in Table 1. In fact, the frequencies of the first and second modes are very weakly influenced by the stiffness of the stabilizing strips (the natural frequency of the first mode varies between 3.9 and 4.1 Hz, while the natural frequency of the second mode remains constant). Differently, mode 3 significantly activates the deformation of the horizontal strips, and such an effect reflects into a 25% variation of the natural frequency of the system (from 9.9 to 12.4 Hz), when passing from strips types A to C (Table 1). By modulating the stiffness of such elements, one is therefore able to significantly tune the frequency associated with the mixed rocking-sliding mode.

3.1.2 | Isolation response

A preliminary set of free-vibration experiments was run to investigate the damping properties of the 2D maglev prototype. The response of the stabilizing strips, in correspondence to small- or moderately-large vibrations of the floating body, is mostly linear-elastic, and therefore, it is assumed to not contribute to any energy dissipation phenomena. The main damping mechanism of the system is associated with the dynamic friction forces acting at the interface between the restraining side-walls and the lateral surface of the levitating platform. These forces depend on several parameters such as relative velocity, contact surface, and normal load, making it difficult to characterize them experimentally. Hence, we have focused on the experimental characterization of damping itself, which translates the ability of the system to dissipate energy. Figure 8 shows the horizontal acceleration record of the free-vibration experiment on the maglev prototype equipped with type A stabilization strips. In this experiment, an initial 10 mm horizontal displacement was applied on top of the cylinder and next the system was left to vibrate freely. No acceleration history was applied to the shake-table. By determining the logarithmic decrements of the acceleration response over a series of cycles of free vibration, it is possible to estimate the damping coefficient of the system.[21] The critical damping ratio showed to be essentially insensitive to the nature of the stabilizing strips, exhibiting an average value of 9.3%. The system was excited with a frequency of about 3.5 Hz, which corresponds to the first mode (Table 1).

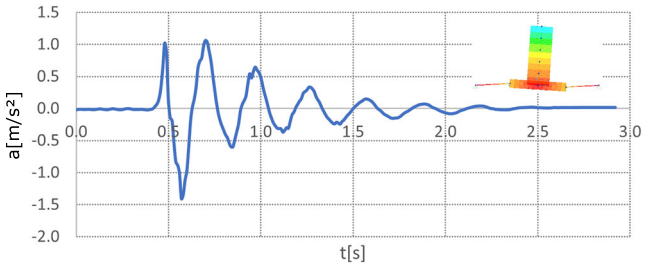

FIGURE 8 Horizontal acceleration record for the free-vibration test on the 2D maglev prototype equipped with type A strips

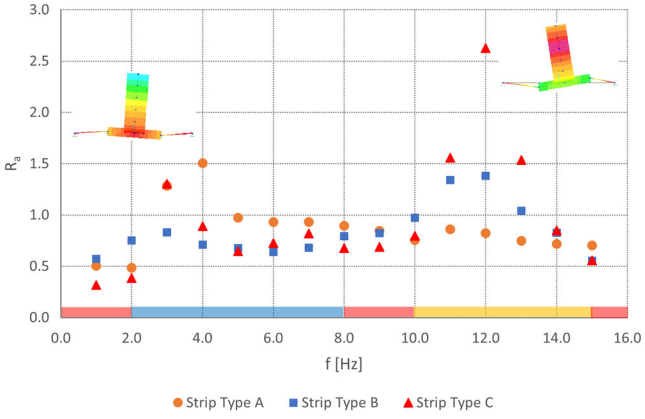

FIGURE 9 Horizontal acceleration ratio $R_a = a_t/a_b$ of the 2D system as a function of input frequency f

We next focused on free-vibration tests. The 2D maglev system was subjected to shake-table tests with harmonic acceleration excitations, sweeping frequency values ranging from 1 to 15 Hz, with 1 Hz increment. The results of such tests are illustrated in Figure 9, which shows the variation with f of the ratio R_a between the maximum amplitude of the steady-state horizontal acceleration recorded at the top of the floating cylinder a_t (absolute value) and the maximum amplitude of the acceleration a_b applied at the base of the prototype (absolute value). Such a ratio was experimentally determined once the system was stabilized.

The results in Figure 9 demonstrate that mode 1 is excited by forcing the system with frequencies between 3.0 and 4.0 Hz, while mode 3 is excited in the presence of input frequencies between 11.0 and 12.0 Hz (see also Movie S1). The color bars placed at the bottom of the R_a versus f plot mark which type of stabilization strips leads to the lowest value of the R_a ratio for a given frequency window. It is possible to acknowledge that the type of strips influences the R_a ratio over all the examined frequency window, especially when mode 1 or mode 3 is dominant. We are led to conclude that it is possible to tailor the dynamic response of the maglev system according to the target value of R_a, for a given frequency range of the expected excitation input (reaching R_a values as low as 0.2).

Figure 9 shows that stabilization strips of type B are particularly suited to mitigate the response of dynamic excitations with frequencies comprised between 3.0 and 7.0 Hz, with mean R_a values of 0.6 (see the blue window in Figure 9), while stabilization strips of type A lead to the lowest R_a values for input frequencies in the range between 11.0 and 14.0 Hz (orange-yellow window). Finally, strips of type C give the best option for either very low frequencies, that is, below 2.0 Hz ($R_a = 0.2$); very high frequencies, equal or greater than 15 Hz ($R_a = 0.5$); or frequencies comprised between 8.0 and 10.0 Hz ($R_a = 0.6$) (red windows).

Figure 10 illustrates the variation with f of the ratio R_{az} between the maximum amplitude of the steady-state vertical acceleration recorded at the top of the floating cylinder a_z (absolute value) and a_b. The plot shown in such a figure highlights that the R_{az} stays generally close to zero. This means that the vertical mode is not appreciably excited by horizontal accelerations at the base and, hence, the horizontal and vertical dynamic responses of the maglev system are mostly decoupled. However, when using stabilization strips of type C, one observes peaks of R_{az} in the frequency window between 10.0 and 14.0 Hz, which leads to $R_{az} = 0.9$. Such peaks are avoided when using stabilization strips of type A or type B. It is worth noting that the above frequency range corresponds to the orange-yellow window in the plot of Figure 9.

3.2 | Results for the 3D system

3.2.1 | Modal analysis

The FE analysis of the 3D maglev system was performed through a simplified model that replaces the statue mock-up with a cylinder showing equal same total mass and height. The first three groups of vibration modes obtained from the FE analysis are presented in Figure 11. Table 1 lists the natural frequencies associated with such modes, for the four and nine magnet pairs configurations. Mode 1 groups the pure rocking vibration motions featuring a pivot point at the center of the levitating platform and arbitrary (horizontal) rotation axis. Mode 2 is a pure vertical motion. Mode 3 groups the family of combined rocking-sliding motions showing arbitrary (horizontal) rotation and sliding axes. When passing from the configuration with four magnet pairs to that with nine magnet pairs, the results presented in Table 2 show that the fundamental frequencies of the 3D maglev system appreciably increase. The same trend is observed when passing from membrane type A to B. Moving from the 4×2 magnet configuration with type A stabilizing membrane to the 9×2 magnet configuration with type B stabilizing membrane, one indeed observes that the modal

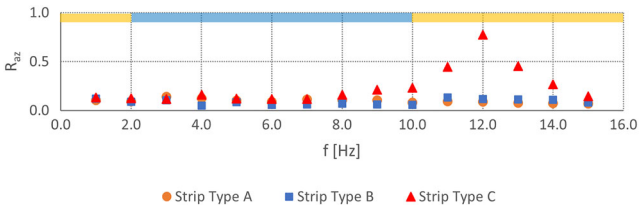

FIGURE 10 Vertical to horizontal acceleration ratio $R_{az} = a_z/a_b$ of the 2D system as a function of input frequency f

vibration frequency increases $\approx 32\%, 40\%$, and 34% for mode 1, mode 2, and mode 3, respectively. Such results highlight that the tuning of the magnetic and stabilizing stiffness of the isolator permits to significantly modulate its vibration behavior.

3.2.2 | Isolation response

Free-vibration experiments were run to investigate the damping properties of the 3D prototype (see Figure 12). A 10 mm initial horizontal displacement was applied to the top of the statue mock-ups, and next the systems were left to vibrate freely (no acceleration histories were applied to the shake-table). By employing the same approach used for the 2D system, we estimated the critical damping ratio of the 3D system, which showed to be essentially insensitive to the number of magnet pairs and membrane type, exhibiting a mean value of 4.9%. The system was excited with a frequency of approximately 2.2 Hz, which corresponds to the natural frequency of the first mode in presence of the four magnet pairs configuration (Table 2). The above damping ratio is lower than that characterizing the 2D system, due to the absence of confinement walls.

Also in the present case, the free-vibration tests were followed by forced excitation tests performed by applying harmonic acceleration histories to the shake-table. We applied excitations with frequencies ranging from 1 to 15 Hz, with 1 Hz steps. The results of such tests are illustrated in Figure 13, which shows the R_a ratio of the current system as a function of the input frequency f.

The results in Figure 13 highlight that mode 1 is excited by forcing the system with frequencies of around 3 Hz, while mode 3 is excited by forcing frequencies comprised in the 9.0–12.0 Hz interval (see also Movie S2). The number of magnets employed in the 3D system, as well as the type of the stabilizing membrane, clearly influences the R_a ratio over the entire examined frequency window. Overall, one observes that the tuning of the magnetic and stabilizing stiffness enables us to tailor the dynamic response of the system according to a target value of R_a, for each given frequency

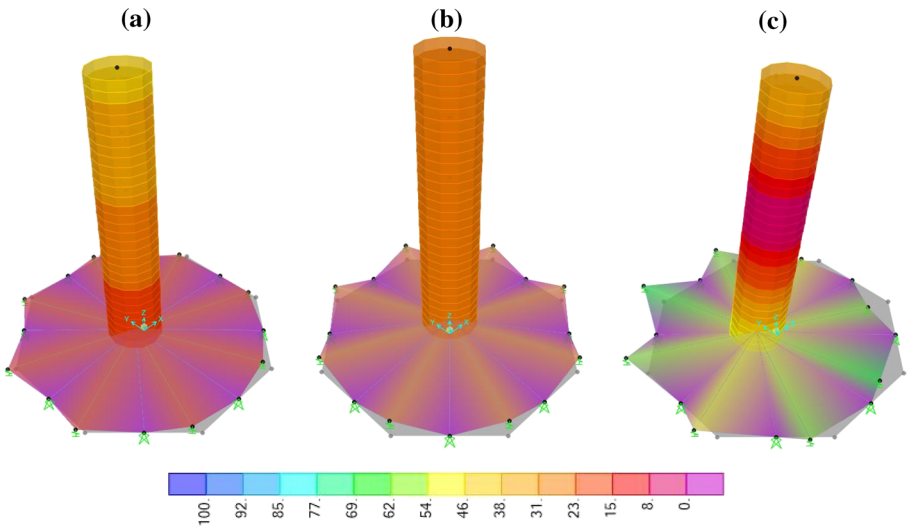

FIGURE 11 Modal configurations for the first three vibration modes of the 3D system. (a) First, rocking mode. (b) Second, vertical mode. (c) Third, mixed rocking-sliding mode

TABLE 2 Natural frequencies associated with the vibration modes in Figure 11

Setting	Mode 1 freq. (Hz)	Mode 2 freq. (Hz)	Mode 3 freq. (Hz)
4 magnets w/ membrane type A	2.2	4.7	7.9
4 magnets w/ membrane type B	2.4	4.7	10.2
9 magnets w/ membrane type A	2.5	6.6	8.8
9 magnets w/ membrane type B	2.9	6.6	10.6

range of the expected excitation (reaching R_a values as low as 0.3). Figure 13 also shows that the configuration with four pairs of magnets with type A membrane is the optimal one, in terms of the mitigation of horizontal vibrations, almost over the entire frequency window 1–15 Hz (look at the red windows in Figure 13, with R_a varying between 0.2 and 0.8), exception made for input frequencies in the range between 8.0 and 10.0 Hz. In such a frequency range, the configuration with nine pairs of magnets becomes optimal (blue window), with a mean value of R_a of 0.8.

Figure 14 shows the dependence of R_{az} of the 3D system on the loading frequency f. One observes that R_{az} stays generally close to zero, as in the 2D case (i.e., the horizontal and vertical dynamic responses of the system are nearly decoupled), with peak values exhibited by the optimized systems not greater than 0.2. However, when using the configuration with four magnet pairs, one observes higher R_{az} peaks near 3 Hz (mode 1 excited) and 9 Hz (mode 3 excited; cf. Table 2).

Finally, we show a comparison of the responses of the 3D system, in terms of accelerations, with and without the isolation feature. Figures 15 and 16 depict the horizontal acceleration time-histories for an input frequency of 5 and 15 Hz, respectively, measured at the top of the statue.

Figures 15 and 16 portrait, in a very clear way, the efficiency of the proposed vibration isolation system, yielding a reduction of the maximum horizontal acceleration amplitudes around 70% and 85%, for the 5 and 15 Hz loading frequencies, respectively.

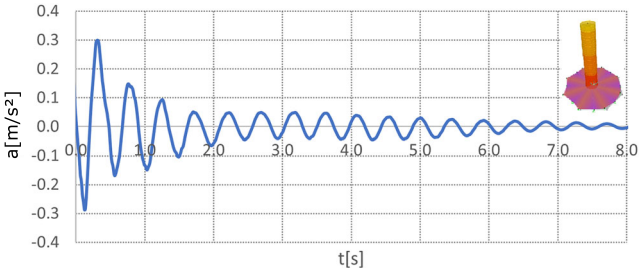

FIGURE 12 Horizontal acceleration record for free-vibration tests on the 3D maglev system

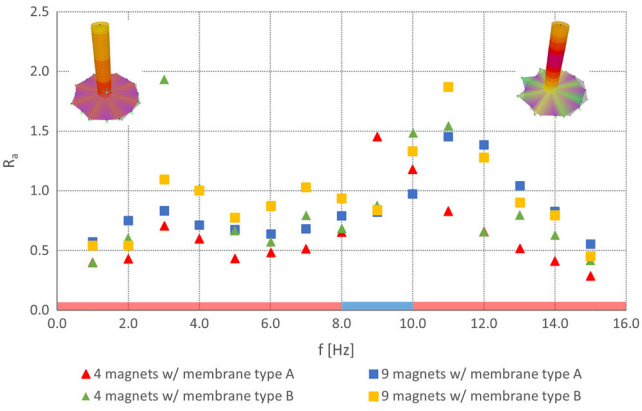

FIGURE 13 Horizontal acceleration ratio $R_a = a_t/a_b$ of the 3D system

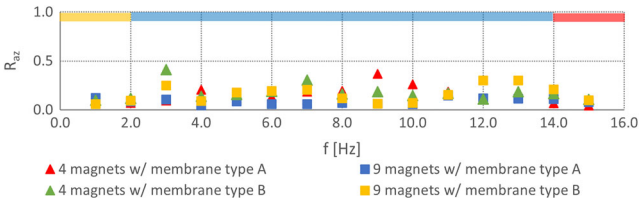

FIGURE 14 Vertical to horizontal acceleration ratio $R_{az} = a_z/a_b$ of the 3D system

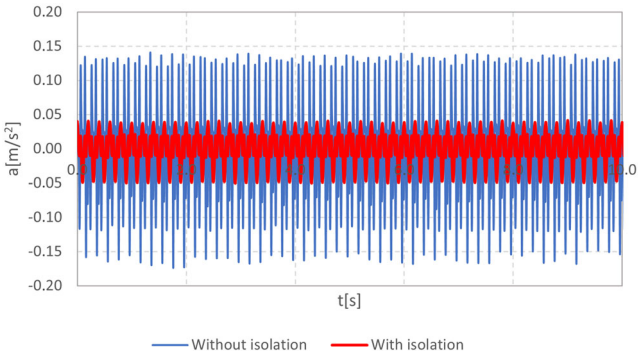

FIGURE 15 Acceleration time-histories for an input frequency of 5 Hz

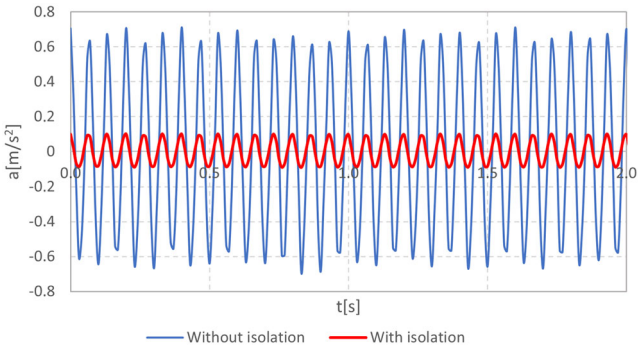

FIGURE 16 Acceleration time-histories for an input frequency of 15 Hz

4 | CONCLUDING REMARKS

The maglev devices examined in the present study employ PMs and 3D-printed parts (3DP maglev), which are low cost and easy to assemble and require ordinary 3D printers. The analyzed systems are effective in damping horizontal vibrations with extremely low stiffness, which implies a very high isolation performance, coupled to an enhanced sensitivity to excitations with very low amplitude. Such behavior is not offered by conventional vibration isolation systems. In addition, the 3DP maglev systems do not require either sub-zero temperatures, like in the case of systems based on superconducting materials, or electrical power, like in electromagnetic-based maglev isolators. As the levitation force is uniquely provided by PMs, a mechanical restraining system is needed to provide the necessary stability of the device. A distinctive feature of the 3DP maglev devices is the possibility to tune the stabilization stiffness through the simple adjustment of the infill density of the 3D-printed parts. In the case of the 2D system, we showed that it is possible to obtain R_a values as low as 0.2. For what concerns the R_{az} ratio, we obtained a mean value of 0.2 over the tested frequency range. Similar results were found for the 3D system. One of the main advantages of the proposed systems is their versatility regarding the design payload. In fact, one can easily control the overall magnetic force developed by the systems simply by changing the number of magnet pairs or, if necessary, by using more powerful magnets. In the tested prototypes, we aimed to obtain a good horizontal stability for the levitating platforms, in the rest position. By using the force–distance relationship shown in Figure 2, it is possible to define the number of magnet pairs according to the weight of the structure and the desired rest position. We can conclude that the 3DP maglev systems analyzed in the present work are tunable, low-cost, passive, eco-friendly isolators, which can be manufactured using materials that are easily accessible around the world. Their development paves the way to a customizable approach to the protection of artworks and lightweight equipment.

In future work, we will address the design and testing of active 3DP maglev isolation systems, which would enable the dynamic control of the degrees of freedom of the device.[22] Additional lines of future research will be aimed at studying the concurrent vibration mitigation performances in the vertical and horizontal directions of maglev isolators, as well as the development of tunable isolation systems that are able to carry payloads significantly larger than those analyzed in the present study.

ACKNOWLEDGMENTS

FF greatly acknowledges financial support through the Italian Ministry of University and Research PRIN 2017 grant 2017J4EAYB. Open Access funding was provided by Università degli Studi di Salerno within the CRUI-CARE Agreement.

CONFLICT OF INTERESTS

The authors declare that they have no conflict of interest.

AUTHOR CONTRIBUTIONS

Conceptualization: FS and FF. *Methodology*: FS and FF. *Investigation*: FS and FF. *Visualization*: FS. *Funding acquisition*: FF. *Project administration*: FS and FF. *Supervision*: FS and FF. *Writing—original draft, and review and editing*: FS and FF.

DATA AVAILABILITY STATEMENT

The FE code employed for the modal analysis of the maglev prototype, as well as the stereolithography (STL) files of all the 3D-printable parts of this prototype, can be provided by the corresponding author upon request.

ORCID

Filipe Amarante dos Santos https://orcid.org/0000-0002-5815-4622
Fernando Fraternali https://orcid.org/0000-0002-7549-6405

REFERENCES

1. Frizenschaf Y, Giles S, Miller J, Pitman T, Stapleton C, Cazzolato B, Robertson W. Development of a magnetic levitation vibration isolator using inclined permanent magnet springs. In: Australian Acoustical Society Conference 2011, Acoustics 2011: Breaking New Ground; 2011:329-336.
2. Guerreiro L, Azevedo J, Muhr AH. Seismic tests and numerical modeling of a rolling-ball isolation system. *J Earthq Eng*. 2007;11(1):49-66.
3. Brancati R, Di Massa G, Pagano S, Petrillo A, Santini S. A combined neural network and model predictive control approach for ball transfer unit-magnetorheological elastomer-based vibration isolation of lightweight structures. *JVC/J Vib Control*. 2020;26(19-20):1668-1682.
4. Li Y, Zi H, Wu X, Zhu L. Flexural wave propagation and vibration isolation characteristics of sandwich plate-type elastic metamaterials. *JVC/J Vib Control*. 2021;27(13-14):1443-1452.
5. Quinteros L, Meruane V, Cardoso EL. Phononic band gap optimization in truss-like cellular structures using smooth p-norm approximations. *Struct Multidiscip Optim*. 2021;64(1):113-124.
6. Venanzi I, Ierimonti L, Materazzi AL. Active base isolation of museum artifacts under seismic excitation. *J Earthq Eng*. 2020;24(3):506-527.
7. Chiozzi A, Simoni M, Tralli A. Base isolation of heavy non-structural monolithic objects at the top of a masonry monumental construction. *Mater Struct/Mater et Constructions*. 2016;49(6):2113-2130.
8. Baggio S, Berto L, Rocca I, Saetta A. Vulnerability assessment and seismic mitigation intervention for artistic assets: from theory to practice. *Eng Struct*. 2018;167:272-286.
9. Fragiadakis M, DiSarno L, Saetta A, et al. Experimental seismic assessment and protection of museum artefacts. In: Proceedings of the International Conference on Structural Dynamic, EURODYN, Vol. 2; 2020:3381-3396.
10. Gidaris I, Taflanidis AA, Lopez-Garcia D, Mavroeidis GP. Multi-objective risk-informed design of floor isolation systems. *Earthq Eng Struct Dyn*. 2016;45(8):1293-1313.
11. Morales E, Filiatrault A, Aref A. Seismic floor isolation using recycled tires for essential buildings in developing countries. *Bull Earthq Eng*. 2018;16(12):6299-6333.
12. Tsuda M, Kojima T, Yagai T, Hamajima T. Vibration characteristics in magnetic levitation type seismic isolation device composed of multiple HTS bulks and permanent magnets. *IEEE Trans Appl Supercond*. 2007;17(2):2059-2062.
13. Tsuda M, Tamashiro K, Sasaki S, Yagai T, Hamajima T, Yamada T, Yasui K. Vibration transmission characteristics against vertical vibration in magnetic levitation type HTS seismic/vibration isolation device. *IEEE Trans Appl Supercond*. 2009;19(3):2249-2252.
14. Sasaki S, Shimada K, Yagai T, Tsuda M, Hamajima T, Kawai N, Yasui K. Suitable shape and arrangement of HTS bulk and permanent magnet for improving levitation force in a magnetic levitation type superconducting seismic isolation device. *IEEE Trans Appl Supercond*. 2010;20(3):985-988.
15. Yao GC, Huang W-C. Performance of a guideway seismic isolator with magnetic springs for precision machinery. *Earthq Eng Struct Dyn*. 2009;38(2):181-203.

16. Diez-Jimenez E, Rizzo R, Gómez-García MJ, Corral-Abad E. Review of passive electromagnetic devices for vibration damping and isolation. *Shock Vib*. 2019;2019:1250707.
17. Perez-Diaz JL, Valiente-Blanco I, Cristache C, Sanchez-García-Casarubios J, Rodriguez F, Esnoz J, Diez-Jimenez E. A novel high temperature eddy current damper with enhanced performance by means of impedance matching. *Smart Mater Struct*. 2019;28:025034.
18. Diez-Jimenez E, AlÉn-Cordero C, Alcover-SÁnchez R, Corral-Abad E. Modelling and test of an integrated magnetic spring-eddy current damper for space applications. *Actuators*. 2019;2021:8.
19. Palagummi S, Yuan F. *Magnetic levitation and its application for low frequency vibration energy harvesting*, Structural Health Monitoring (SHM) in Aerospace Structures; 2016;213-251.
20. Hasegawa T. Challenges toward development of rear-earth free feco based permanent magnet. *Electron Commun Jpn*. 2021;104(2): e12307.
21. Chopra AK. *Dynamics of Structures: Theory and Applications to Earthquake Engineering*. 2nd ed.: Prentice-Hall, Inc.; 2001.
22. Kamaruzaman NA, Robertson WSP, Ghayesh MH, Cazzolato BS, Zander AC. Six degree of freedom quasi-zero stiffness magnetic spring with active control: theoretical analysis of passive versus active stability for vibration isolation. *J Sound Vib*. 2021;502.

SUPPORTING INFORMATION

Additional supporting information may be found in the online version of the article at the publisher's website.

How to cite this article: Amarante dos Santos F, Fraternali F. Novel magnetic levitation systems for the vibration control of lightweight structures and artworks. *Struct Control Health Monit*. 2022;e2973. doi:10.1002/stc.2973